Published in final edited form as:
Bone. 2010 June ; 46(6): 1604–1612. doi:10.1016/j.bone.2010.02.030.

Healing of Non-Displaced Fractures Produced by Fatigue Loading of the Mouse Ulna

Mario D. Martinez[1], **Gregory J. Schmid**[2], **Jennifer A. McKenzie**[1,3], **David M. Ornitz**[2], and **Matthew J. Silva**[1,3]

Mario D. Martinez: mario.d.martinez@gmail.com; Gregory J. Schmid: gschmid@stanford.edu; Jennifer A. McKenzie: mckenziej@wudosis.wustl.edu; David M. Ornitz: dornitz@wustl.edu; Matthew J. Silva: silvam@wustl.edu

[1] Department of Orthopaedic Surgery, Washington University, St. Louis, Missouri

[2] Department of Developmental Biology, Washington University, St. Louis, Missouri

[3] Department of Biomedical Engineering, Washington University, St. Louis, Missouri

Abstract

We developed a fatigue loading protocol in mice to produce a non-displaced ulnar fracture in vivo, and characterized the early healing response. Using adult (5 mo) C57Bl/6 mice, we first determined that cyclic compression of the forelimb under load-control leads to increasing applied displacement and, eventually, complete fracture. We then subjected the right forelimbs of 80 mice to cyclic loading (2 Hz; peak force ~4 N) and limited the displacement to 0.75 mm (60% of the average displacement at complete fracture). This fatigue protocol created a partial, non-displaced fracture through the medial cortex near the ulnar mid-shaft, and reduced ulnar strength and stiffness by >50%. Within 1 day, there was significant upregulation of genes related to hypoxia (*Hif1a*) and osteogenesis (*Bmp2*, *Bsp*) in loaded ulnae compared to non-loaded, contralateral controls. The gene expression response peaked in magnitude near day 7 (e.g., *Osx* upregulated 8-fold), and included upregulation of FGF-family genes (e.g., *Fgfr3* up 6-fold). Histologically, a localized periosteal response was seen at the site of the fracture; by day 7 there was abundant periosteal woven bone surrounding a region of cartilage. From days 7 to 14, the woven bone became denser but did not increase in area. By day 14, the woven-bone response resulted in complete recovery of ulnar strength and stiffness, restoring mechanical properties to normal levels. In the future, the fatigue loading approach can be used create non-displaced bone fractures in transgenic and knockout mice to study the mechanisms by which the skeleton rapidly repairs damage.

Keywords

fracture healing; fatigue loading; mouse ulna; FGF signaling; woven bone; hypoxia

Correspondence to: Matthew J. Silva, Ph.D., Department of Orthopaedic Surgery, Washington University School of Medicine, 1 Barnes-Jewish Hospital Plaza, Suite 11300 WP, St. Louis, Missouri 63110, silvam@wustl.edu, Telephone: (314) 362-8585, FAX: (314) 362-0334.

The authors report no conflicts of interest.

Introduction

Bone has a remarkable capacity for self-repair of injuries of varying degree. Severe bone injuries involve complete fracture with displacement of the fractured ends. If appropriately stabilized, healing of displaced fractures occurs by a complex process of endochondral ossification at the fracture site and adjacent intramembranous ossification. This process is controlled by the coordinated temporospatial expression of multiple genes supporting angiogenesis, osteogenesis and chondrogenesis [1–3]. For example, the documented increase in expression of hypoxia-inducible factor-1 (*Hif1α*) and vascular endothelial growth factor (*Vegf*) likely play a role in angiogenesis [4], while upregulation of bone morphogenetic protein-2 (*Bmp2*) and osterix (*Osx*) play a role in bone formation [5–7], and upregulation of type 2 collagen (*Col2a1*) plays a role in chondrogenesis [6–9]. Moreover, expression of several fibroblast growth factors (*Fgfs*) and their receptors (*Fgfrs*) are increased during fracture healing, suggesting a functional role for FGFs in skeletal repair [10–14]. FGFs can differentially regulate angiogenesis, osteogenesis and chondrogenesis [15–17].

Most animal studies of fracture healing utilize a closed, blunt trauma model whereby three-point bending produces a displaced fracture [18]. This model requires placement of an intramedullary rod to stabilize the fracture, making it an excellent model of displaced fractures requiring internal fixation. This model was first described for rats, but has been applied to mice in the past decade [6–8,9,14,19–21]. Recovery of bone strength occurs in approximately 5 weeks after fracture of the mouse femur and tibia [19–21]. One limitation of the blunt trauma model is that it does not allow studies of less severe injuries, i.e., partial or non-displaced fractures. Non-displaced fractures can be simulated using osteotomy followed by rigid internal fixation [22], although this approach requires surgical intervention.

An approach for creating controlled bone injuries in animals without surgical intervention is through use of fatigue loading. Repetitive compression of the rat forelimb has been used to create ulnar stress fractures in vivo [23–26]. These stress fractures appear as oblique, non-displaced cracks that initiate at the periosteal surface and extend partially through the cortex. The early response to a stress fracture in this model is characterized by the rapid production of sub-periosteal woven bone without cartilage, leading to stabilization of the fracture with recovery of mechanical properties within 2 weeks [25,27–29]. By day 10 after stress fracture osteoclasts are seen intracortically [28,30], and the cracks are eventually repaired via direct remodeling [24,27]. Recent reports have described the molecular responses following a stress fracture in the rat ulna, and have noted many similarities to fracture healing [24,31]. Some common features include early upregulation of *Bmp2* and *Vegf* [31], and a sharp increase in *Col2a1* expression at 7 days post-injury, despite the negligible cartilage observed in the stress fracture model [24]. These findings indicate that across a range of bone injuries, from stress fractures to displaced fractures, there are common features of repair.

To advance our understanding of the mechanisms that control bone repair across a range of injury severities, we sought to develop a model to produce controlled fractures in mice. The first objective of this study was to develop a fatigue loading protocol for the mouse forelimb that generates a partial, non-displaced ulnar fracture. Our second objective was to describe the early molecular and histological responses to this fracture and the related changes in densitometric and mechanical properties. We hypothesized that non-displaced fractures heal by a process that has features common to both more severe complete fractures and less severe stress fractures.

Methods

Animals

Male C57Bl/6 mice were obtained at 3 months from Harlan (in batches of 10–15) and aged in our animal facility until use at 4.5–5.5 mo. At this age mice have completed their rapid skeletal growth phase and are skeletally mature [32]. Forelimbs were loaded in vivo by axial compression similar to previous studies [33–34]. In brief, mice were anesthetized (1–3% isofluorane) and forelimbs were positioned in loading fixtures attached to a servohydraulic materials testing machine (Instron 8841 outfitted with 25 lb Lebow load cell). A 0.3 N pre-load was applied. Fatigue loading was performed at 2 Hz (hsine) under load-control (i.e., same peak force for each load cycle), based on our previous approach in the rat [26]. Force and displacement data were collected at 60 Hz (Labview, National Instruments). Immediately after loading, survival mice were administered buprenorphine hydrochloride (0.1mg/kg, i.m.) for analgesia. Mice were then allowed free cage activity and given a standard laboratory diet ad libitum. Mice showed no signs of decreased activity or lameness. Mice were euthanized by CO_2 asphyxiation at their designated timepoints. All procedures were approved by our institutional Animal Studies Committee.

Monotonic loading to complete fracture

Both forelimbs of five mice were loaded by a displacement ramp (0.5 mm/sec) to complete, displaced fracture in order to determine monotonic mechanical properties. Mice were euthanized immediately after loading. Ultimate force (mean ± SD) was 4.32 ± 0.21 N, and stiffness was 3.98 ± 0.26 N/mm.

Fatigue loading to complete fracture

Both forelimbs of 14 mice were cyclically loaded at peak compressive forces (F) ranging from 2.1 to 3.5 N (50 to 80% of average ultimate force) until complete fracture. Cycles to failure (N_f) were recorded. Mice were euthanized immediately after fracture. Ten forelimbs from 7 mice were excluded either because they did not fracture within 6 hours (n = 5) or because of technical errors (n = 5). A highly significant fatigue-life relationship was obtained: $F/F_{ult} = -0.077*\log(N_f) + 0.993$ ($r^2 = 0.93$, $p < 0.05$). From this, we estimated that a peak force of 72% of ultimate force would produce complete fracture in an average of 3600 cycles (30 min).

Displacement data were analyzed to determine peak (maximum) actuator displacement for each cycle, and from these values we determined the increase in peak actuator displacement from cycle 10 to fracture. (We use cycle 10 as a reference because there is substantial soft tissue pre-conditioning during the first few cycles.) We previously found that this parameter provides a reliable indicator of when complete fracture occurs during cyclic loading, independent of peak force [26]. The average increase in peak displacement to fracture for the mouse forelimbs was 1.25 ± 0.32 mm (Fig. 1).

Batch calibration

In preliminary studies we observed large variation in forelimb ultimate force between batches of mice, but small variation within batches. Thus, prior to survival experiments, one or two mice from each batch (n=13; 7 batches total) were used to estimate failure properties for the batch. One forelimb was loaded monotonically to determine ultimate force, the other forelimb was fatigue loaded to determine displacement to fracture. Average ultimate force for the batches used in survival experiments was 5.42 ± 0.37 N, different from the original batch (above). Average displacement increase to fracture was 1.31 ± 0.45 mm, similar to the original batch.

Fatigue loading to partial, non-displaced fracture

Right forelimbs of 80 mice were cyclically loaded at peak forces ranging from 3.75 to 4.10 N (70–75% of ultimate force) while displacement was monitored. Loading was terminated when peak displacement increased by 0.75 mm relative to the peak displacement at cycle 10. (Relative to the minimum displacement at cycle 10, the total displacement increase was 1.23 ± 0.04 mm.) The increase of 0.75 mm corresponded to 60% of the average increase in peak displacement to complete fracture (Fig. 1). This criterion was based on our previous rat study, wherein cyclic loading of forelimbs to 60% of fracture produced an ulnar stress fracture and a loss of strength of 40% [26]. Two mice sustained complete fractures during loading; they were euthanized and excluded. Left forelimbs were not loaded and were used as contralateral controls. Bilateral ulnae were harvested for analysis from 0 to 14 days after loading (Table 1).

Gene expression by qRT PCR

Expression of 15 target genes was assessed by quantitative, real-time RT-PCR. Mice were euthanized at one of five timepoints: 1 hour; 1, 3, 7 and 11 days after loading (n = 4–5). Immediately post mortem, right and left ulnae were dissected and frozen in liquid nitrogen. The ends of each ulna were removed and the central 7 mm (mass: 7.22 ± 1.14 mg) was stored at −80°C. Total RNA was isolated using a standard approach described in detail previously [31]. Briefly, each sample was pulverized to powder in a liquid nitrogen-cooled stainless steel shaking flask (Mikro-Dismembrator, B. Braun Biotech Inc.). RNA was stabilized with TRIzol reagent (Invitrogen) and isolated using a chloroform extraction. RNA was purified using the RNeasy Mini Kit (Qiagen). Potential DNA contamination was eliminated using an on-column RNase-Free DNase Set (Qiagen) and RNA concentration was measured (Nanodrop). First strand cDNA was synthesized using Superscript III DNA First Strand Synthesis System (Invitrogen) per manufacturer's instructions. Either 250 or 500 ng of RNA was used as starting material for the reactions, depending on initial RNA concentration. cDNA was eluted in 20 μL of H_20 and diluted to a final volume of either 60.25 μL (for 250 ng) or 120.5 μL (for 500 ng).

Gene expression was then quantified using Taqman Gene Expression Assays (Applied Biosystems) and an ABS7500 Fast Thermocycler set to the following program: 95°C for 20 s, followed by 45 cycles of 95°C for 3 s, and 60°C for 30 s [14]. Fifteen genes were selected based on their reported roles in fracture healing [4,6–7,9,14] or stress fracture healing [31], with a focus on osteogenesis, angiogenesis, and FGF ligands and receptors (Table 2). Expression of each target gene was normalized to the housekeeping gene *Hprt* (ΔCt). Expression in the loaded limbs was then normalized relative to the respective contralateral control ulna to determine fold change in local expression due to loading ($2^{-\Delta\Delta Ct}$).

Histology

The ulnar response was assessed using routine histology. Mice were euthanized at one of five timepoints: 1 hour; 1, 3, 7 and 11 days after loading (n = 3). Ulnae were dissected, fixed in 10% formalin overnight (4°C), decalcified in 14% EDTA for 4–5 weeks, and embedded in paraffin. Longitudinal or transverse sections (5 μm thick) were cut and stained with hematoxylin & eosin (H&E). Sections were visualized under bright field using a 10x objective (Olympus BX51) and imaged (Olympus DP70).

MicroCT

All ulnae (N = 39) assigned to histomorphometry and mechanical testing were first imaged using micro-computed tomography (Scanco μCT40, 16 μm resolution). Bone area (B.Ar) and volumetric mineral density (BMD) were determined using the manufacturer's software at nine sites along the ulna, from 1 mm proximal to the midpoint (P1) to 3 mm distal to the midpoint

(D3) at 0.5 mm intervals. The periosteal and endosteal margins of the ulna were defined by manual contouring; the region of interest included pre-existing cortical bone and any new woven bone, but not the marrow cavity (unless filled with woven bone). Images were also analyzed for the presence and location of a crack (fracture) and the longitudinal extent of woven bone. Two 14-day samples were not analyzed because they had a displaced fracture.

Histomorphometry

Bone formation and morphology were assessed using standard techniques. Calcein green (10 mg/kg, Sigma) and alizarin complexone (30 mg/kg, Sigma) were administered by i.p. injection 7 and 2 days prior to death, respectively. Mice were euthanized 7 or 14 days after loading (n = 8 each). Right and left ulnae were dissected, fixed in 10% formalin overnight (4°C), and stored in 70% ethanol (4°C), until microCT scanning. Samples were then dehydrated in increasing ethanol concentrations (70% to 100%) followed by xylene, and then infiltrated and embedded in methylmethacrylate. Three sections (80–100 μm thick) per bone were cut between the midpoint (MP) and 1 mm distal to the midpoint (D1) (Leica SP 1600). Sections were mounted on glass slides, ground to 30–35 μm thickness, and visualized at 10X objective using a fluorescent microscope (Olympus IX51). Calcein and alizarin were visualized using FITC and TRITC filters, respectively. Images were digitized (Olympus DP70), merged, and analyzed (Bioquant). We determined woven bone area, total bone area (woven plus original cortical), single-labeled surface, double-labeled surface, woven bone-labeled surface and non-labeled surface. Values were averaged over three sections per ulna.

Mechanical testing

Ulnar mechanical properties were determined by three-point bending. Mice were euthanized at day 0 (just after fatigue loading; n = 10) or day 14 (n =13). Right and left ulnae were dissected and stored at −20°C. After microCT scanning, three point-bending tests were performed at room temperature. Ulnae were positioned on supports 10 mm apart, and loaded by a transverse force applied at the mid-span at 0.5 mm/s to failure. Ultimate moment, rigidity, post-yield displacement and energy to fracture were determined from force-displacement plots. Two 14-day samples were not analyzed because they had a displaced fracture seen on microCT.

Data analysis

Differences between loaded (right) and non-loaded control (left) ulnae were assessed using paired t-tests at each timepoint. Analysis of variance (ANOVA) was used to the effect of time; differences between individual timepoints were assessed using Fisher's protected least significant difference test. Significance was defined as $p < 0.05$.

Results

Day 0: Creation of non-displaced fracture

Fatigue loading to 60% of fracture displacement produced a partial, non-displaced fracture (crack) of the ulna visible by microCT (10 of 10 samples; Fig. 2A) and histology (not shown). The fracture was located on the medial side of the ulna near the midpoint, between sections MP and D1, with a longitudinal extent of 0.38 ± 0.14 mm. Although the fatigue-loaded ulnae remained intact, three-point bending revealed a dramatic loss of mechanical properties (Table 3). Ultimate moment (a measure of strength) was 53% less in loaded vs. control ulnae, while rigidity (a measure of stiffness) was 77% less (Fig. 3). One hour after loading, there were no significant changes in the expression of any target genes (Table 4).

Day 1: Initial molecular response

One day after loading, a small but significant increase was observed in the expression of genes associated with angiogenesis and osteogenesis (Table 4). The bone morphogen *Bmp2* was upregulated by 2-fold in loaded vs. control ulnae, as was the hypoxia-sensitive gene *Hif1a*, both of which have been identified as angiogenic-osteogenic coupling factors [35–36]. Additionally, the bone mineralization regulator *Bsp*, shown to be an early responder after fatigue loading in rats [31], was upregulated 3-fold in loaded ulnae (Fig. 4A). Histologically, the medial periosteum was elevated and a fibrin clot was evident; an oblique fracture was seen through the medial cortex (Fig. 5).

Day 3: Increased expression of genes associated with skeletal repair

By 3 days post loading, a robust molecular response was observed, with 8 of 15 target genes significantly upregulated (Table 4). *Hif1a* expression increased to 3-fold in loaded ulnae vs. control, indicative of continued hypoxia, although the angiogenic factor *Vegfa* was not upregulated (Fig. 4A). There was significant upregulation of genes associated with osteogenesis including *Bsp* (9-fold), *Osx* (3-fold) and *Col1a1* (2-fold). Genes in the FGF family were also upregulated, with the three receptors (*Fgfr1*, *Fgfr2*, *Fgfr3*) and the ligand *Fgf18* approximately 2-fold higher in loaded ulnae vs. control (Fig. 4B). Histologically, there appeared to be increased cellularity and vascularity at the fracture site. The medial periosteum was expanded by the presence of loose fibrovascular tissue, while sub-periosteally there was some osteoid deposition.

Day 7: Continued upregulation of skeletal repair genes; formation of cartilage and low-density woven bone

Seven days after loading the robust molecular response persisted; 10 of 15 target genes were significantly upregulated, several at their maximal levels compared to other timepoints (Table 4; Fig. 4). *Hif1a* remained elevated by ~3-fold. Osteogenic genes *Bmp2*, *Bsp* and *Osx* were significantly upregulated in loaded ulnae vs. control, with *Bsp* (33-fold) and *Osx* (8-fold) at their maximal values. The cartilage matrix gene *Col2a1* was upregulated for the first time, by 360-fold. (Normalized expression levels [right/left] for *Col2a1* ranged from 32 to 1091 for the five samples at this timepoint.) The three FGF receptors were upregulated to their maximal levels, and the ligands *Fgf16* and *Fgf18* were also upregulated.

Abundant new woven bone was evident by microCT (Fig. 2A) and histologically (Fig. 2B; Fig. 5). It was observed on both the lateral and medial surfaces of the ulna, although it was thickest medially. The longitudinal extent of woven bone was 2.4 ± 0.7 mm. In one of three histological samples, cartilage was seen in the center of the woven bone. Histomorphometric analysis indicated significantly increased bone area near the ulnar midpoint due to the addition of woven bone, which covered more than 50% of the bone cross-section (Table 5). Quantitative analysis of microCT images over the central one-third of the ulna showed a pattern of increase in bone area centered at section D1 (Fig. 6). Volumetric BMD was decreased over the same region, consistent with the addition of low-density woven bone.

Days 11–14: Decrease in osteogenic gene expression, densification of woven bone, and recovery of ulnar strength and stiffness

The expression of most target genes continued to be upregulated in loaded ulnae vs. control on day 11, although genes associated with osteogenesis (*Bsp*, *Osx*) were decreased relative to day 7 (Table 4). *Col2a1* expression was greatly reduced although still 6-fold higher than control (Fig. 4A). *Fgfr3* levels decreased from day 7 to 11, whereas *Fgf9* and *Fgf18* were at their maximal values (Fig. 4B).

Histologically, a relatively compact woven bone callus was observed over the periosteal surface of loaded ulnae on days 11 (Fig. 5) and 14 (Fig. 2). In one of three samples there was cartilage in the center of the woven bone callus on day 11. (In one other sample there was a displaced fracture with exuberant soft callus.) The longitudinal extent of woven bone was 2.5 ± 0.8 mm. Quantitative histomorphometric (Table 5) and microCT (Fig. 7) analyses found no significant increase in woven bone or total bone area from 7 to 14 days. The volumetric BMD of the loaded ulnae remained less than normal, although in the region between MP and D2 there was an increase in BMD from 7 to 14 days ($p = 0.043$), consistent with decreased porosity in the woven bone layer.

Three-point bending revealed complete recovery of ulnar mechanical properties. Ultimate moment, rigidity and fracture energy of loaded ulnae were not different from control on day 14 ($p > 0.05$), whereas these parameters were significantly reduced in loaded ulnae vs. control on day 0 (Fig. 3; Table 3).

Discussion

We developed a fatigue loading protocol for the mouse forelimb that generates a non-displaced ulnar fracture, and characterized the early healing response. First, we confirmed that cyclic compression of the mouse forelimb under load-control leads to progressively increasing applied displacement and, eventually, complete fracture. If the displacement is limited to 60% of the displacement at complete fracture, a non-displaced fracture is observed through the medial cortex near the ulnar mid-shaft. The ulna remains intact, although its strength and stiffness are reduced by greater than 50%. Within 1 day after fracture, there is significant upregulation of genes related to hypoxia and osteogenesis. The gene expression response peaks in magnitude near day 7 and includes upregulation of the cartilage marker *Col2a1* and genes in the FGF family. Histologically, localized periosteal and endosteal responses are seen at the fracture site, and by day 7 there is often cartilage at the periosteal fracture site surrounded by woven bone. From days 7 to 14, the woven bone becomes denser but does not increase in area. By day 14, the woven-bone response results in complete recovery of ulnar strength and stiffness.

The method we describe for producing a non-displaced fracture provides a new approach to study bone healing in mice. This method is non-invasive and complements previous murine studies that have utilized blunt trauma (with medullary pin stabilization) to produce a complete (i.e., both cortices) fracture with displaced ends [6–8,9,14,19–21]. Our approach is based on studies of fatigue loading in rats [23,25–26,28], and utilizes the increase in forelimb displacement during loading as an indicator of ulnar damage [26]. Cyclic loading of the rat forelimb (~18 N peak force) to 85% of fracture displacement resulted in a non-displaced fracture localized to the medial cortex of the ulna and an associated loss of ulnar strength and stiffness of 55 and 80%, respectively [26]. Because the fracture in the rat ulna was partial and non-displaced, and because the repair process involved negligible cartilage formation, we referred to this as a “stress fracture”, consistent with descriptions by others [23–25]. For cyclic loading of the mouse forelimb, we reduced the peak force (~4 N) and displacement limit to account for the much weaker and smaller structure, but the loading protocol was otherwise similar. We observed that loading the mouse forelimb to 60% of fracture displacement resulted in a partial, non-displaced fracture, with loss of ulnar stiffness and strength of 53 and 77%, respectively, similar to the previous rat study. Yet examination of the fracture morphology indicated a more severe bone injury in the current study. The fracture extended through the medial cortex and there was sometimes evidence of damage in the lateral cortex. In future studies, a more moderate level of damage could be produced by lowering the displacement limit; we expect that with this modification our approach could be used to create a more limited “stress fracture” that does not extend though the entire cortex.

In the first 2 weeks following creation of a non-displaced fracture, we observed a modified fracture healing response. Cartilage was often observed at 7 and 11 day timepoints and appeared only on the medial surface, corresponding to the periosteal fracture location. By comparison, in studies of complete fracture in mice cartilage is seen on both sides of the bone as well as between the fractured ends [8–9]. In studies of stress fracture healing in rats, a very small island of cartilage is observed on day 7 where the crack intersects the periosteum [24,31]. Consistent with chondrogenesis in the current study, there was a sharp increase from 3 to 7 days in expression of *Col2a1*, and then a sharp decline from 7 to 11 days. The timing of the increase in *Col2a1* expression matches what has been reported in fracture healing in mice [7–9]. Interestingly, a similar sharp increase in *Col2a1* expression was reported in a rat stress fracture study [24], despite the fact that the crack extent was localized to the medial cortex and there was negligible cartilage formation.

The molecular response to non-displaced fracture included early upregulation of *Bmp2* and *Hif1a. Bmp2* was upregulated by approximately 2-fold on days 1, 7 and 11. A similar early and sustained elevation of *Bmp2* was reported after both stress fracture [24,31] and complete fracture [6]. BMP2 is required for fracture healing [37], and early upregulation of *Bmp2* may trigger subsequent osteogenesis as well as angiogenesis [31,35]. Related to vascularity, we also observed upregulation of the hypoxia factor *Hif1a*, which reached a peak of 3-fold on days 3 and 7. In healing of complete fractures, both *Hif1a* and its downstream target *Vegf* increased to peak levels 10 days after fracture [4]. The slightly later peak of *Hif1a* after complete fracture likely reflects the greater extent of injury compared to the current study. However, we cannot explain the lack of a VEGF response in the current study in light of the fracture healing results [4] and other evidence of a strong linkage between HIF1a and VEGF in bone angiogenesis and osteogenesis [36,38].

The predominant histological response in our study was the direct formation of a hard callus of woven bone, which appeared between days 3 and 7. Bone formation was preceded by increases in *Bsp* (first up significantly on day 1) and *Osx* (up on day 3). Expression of these osteogenic-related genes peaked on day 7. Consistent with these findings, we previously noted upregulation of *Bsp* and *Osx* within 1 day after stress fracture with peak values attained 3 to 7 days after injury [31]. After complete fracture, *Bsp* expression is reported to peak on day 10 [3] while *Osx* peaks on day 14 [7], slightly later than occurred in the current study. The spatial distribution of new woven bone in the mouse ulna corresponded to the location of the non-displaced fracture, in a pattern that is similar to that observed in stress fracture healing [31]. Overall, the osteogenic response after a non-displaced fracture is similar to the response after a stress fracture, while it differs slightly from the response seen in healing of complete fractures. The main difference in osteogenesis in a non-displaced fracture versus a complete fracture is that the expression of osteogenic genes peaks earlier in the non-displaced fracture, consistent with the greater relative amount of intramembranous versus endochondral ossification.

FGFs and FGFRs are important in both chondrogenesis and osteogenesis. Consistent with our finding of chondrogenesis after non-displaced fracture, *Fgfr3* expression was significantly upregulated at day 7 and 11. FGF18 functions to negatively regulate chondrogenesis through FGFR3 and positively regulate osteogenesis through other FGFRs [16]. The relatively uniform upregulation of FGF18 throughout the stress fracture healing period may reflect both of these processes, an initial osteogenic response and a later chondrogenic response. Similar to what was seen during fracture repair in mice [14], FGF18 expression increased from day 7 to 11 after non-displaced fracture, consistent with a decrease in *Col2a1* expression and diminished chondrogenesis. The function of FGF16 in skeletal development has not yet been defined, however the significant increase in *Fgf16* in both the complete fracture model [14] and the non-displaced model presented here suggests a function in skeletal response to injury. In the non-displaced fracture model, *Fgf2* showed very little change in expression over the 11 days

of the experiment. This is in sharp contrast to the complete fracture model, where *Fgf2* was rapidly upregulated within one day post fracture. A notable difference between the two models is that in the complete fracture model, a tibial pin is inserted, whereas in the non-displaced fracture model the bone marrow space is not violated. Insertion of a tibial pin by itself results in rapid upregulation of *Fgf2* in response to injury to the bone marrow.

The ulna recovered its load-bearing capacity rapidly after non-displaced fracture. Despite the acute loss of strength and stiffness of more than 50% on day 0 after fatigue loading, these properties were not different from control on day 14. The timing of strength recovery is the same as reported in previous studies of stress fracture healing in the rat ulna [27–29], and is consistent with the rapid formation of periosteal woven bone in both cases. In slight contrast, strength recovery takes approximately 5 weeks after complete fracture of a mouse long bone [19–21]. The longer time to healing for a complete fracture is consistent with the greater level of damage and the greater relative amount of endochondral ossification.

Our study has several limitations. The level of ulnar damage created by our loading protocol was high. As a result, there were several inadvertent fractures, although these were easily detected during microCT or histological review. Another limitation relates to the small size of the affected region of the ulna. We used the central 7 mm length for RNA isolation to ensure adequate yield. But because the average woven bone extent was only 2.5 mm, the mRNA from the site of interest was effectively diluted by mRNA from adjacent, non-injured bone. This may have resulted in a lower signal: noise for gene expression in our study as compared to studies of complete fracture healing, which have a larger region of response [14]. This issue may be overcome in the future by using a smaller length of ulna but pooling RNA from multiple bones. Another limitation is that we used the contralateral, non-loaded ulna as a control and thus our findings reflect only the local effects of loading. It is possible that there were also systemic effects of loading, as has been reported in some [24,39] (but not all [40]) studies of bone loading. To evaluate the possible effect this may have had on gene expression, we compared the expression of genes in loaded ulnae to a small set (n = 4) of ulnae from age-matched mice. Importantly, the fold difference values we determined when comparing loaded vs. normal control were not notably different from the results of loaded vs. contralateral control. One advantage in comparing paired samples from the same animal is increased statistical power.

In summary, we developed a non-displaced fracture model in the mouse. Application of displacement-limited, cyclic compression to the mouse forelimb produced a unicortical fracture at the ulnar mid-shaft leading to acute loss of stiffness and strength. After fracture creation, there was a robust upregulation of genes related to hypoxia, osteogenesis, chondrogenesis and FGF signaling. Within 1 week there was abundant woven bone formation surrounding a small region of cartilage centered at the periosteal fracture, and within 2 weeks the mechanical properties of the ulna had recovered to normal. The healing response to the non-displaced fracture had features common to both more severe complete fractures and less severe stress fractures. We believe that the non-displaced fracture model represents an intermediate point on the continuum of bone injury and offers an alternate, non-invasive approach to study bone repair. In the future, this model can be used in transgenic and knockout mice to extend our understanding of the mechanisms by which the skeleton rapidly repairs injuries of varying severity.

Supplementary Material

Refer to Web version on PubMed Central for supplementary material.

Acknowledgments

This study was supported by grants from the NIH (R01AR050211, R01HD049808, P30AR057235) and the ASBMR. We thank C. Smith for technical assistance.

References

1. Ai-Aql ZS, Alagl AS, Graves DT, Gerstenfeld LC, Einhorn TA. Molecular mechanisms controlling bone formation during fracture healing and distraction osteogenesis. J Dent Res 2008;87:107–18. [PubMed: 18218835]
2. Gerstenfeld LC, Cullinane DM, Barnes GL, Graves DT, Einhorn TA. Fracture healing as a post-natal developmental process: molecular, spatial, and temporal aspects of its regulation. J Cell Biochem 2003;88:873–84. [PubMed: 12616527]
3. Hadjiargyrou M, Lombardo F, Zhao S, Ahrens W, Joo J, Ahn H, et al. Transcriptional profiling of bone regeneration. Insight into the molecular complexity of wound repair. J Biol Chem 2002;277:30177–82. [PubMed: 12055193]
4. Komatsu DE, Hadjiargyrou M. Activation of the transcription factor HIF-1 and its target genes, VEGF, HO-1, iNOS, during fracture repair. Bone 2004;34:680–8. [PubMed: 15050899]
5. Bostrom MP, Lane JM, Berberian WS, Missri AA, Tomin E, Weiland A, et al. Immunolocalization and expression of bone morphogenetic proteins 2 and 4 in fracture healing. J Orthop Res 1995;13:357–67. [PubMed: 7602397]
6. Cho TJ, Gerstenfeld LC, Einhorn TA. Differential temporal expression of members of the transforming growth factor beta superfamily during murine fracture healing. J Bone Miner Res 2002;17:513–20. [PubMed: 11874242]
7. Kaback LA, Soung do Y, Naik A, Smith N, Schwarz EM, O'Keefe RJ, et al. Osterix/Sp7 regulates mesenchymal stem cell mediated endochondral ossification. J Cell Physiol 2008;214:173–82. [PubMed: 17579353]
8. Kon T, Cho TJ, Aizawa T, Yamazaki M, Nooh N, Graves D, et al. Expression of osteoprotegerin, receptor activator of NF-kappaB ligand (osteoprotegerin ligand) and related proinflammatory cytokines during fracture healing. J Bone Miner Res 2001;16:1004–14. [PubMed: 11393777]
9. Sakano S, Zhu Y, Sandell LJ. Cartilage-derived retinoic acid-sensitive protein and type II collagen expression during fracture healing are potential targets for Sox9 regulation. J Bone Miner Res 1999;14:1891–901. [PubMed: 10571689]
10. Nakajima F, Ogasawara A, Goto K, Moriya H, Ninomiya Y, Einhorn TA, et al. Spatial and temporal gene expression in chondrogenesis during fracture healing and the effects of basic fibroblast growth factor. J Orthop Res 2001;19:935–44. [PubMed: 11562144]
11. Nakajima A, Nakajima F, Shimizu S, Ogasawara A, Wanaka A, Moriya H, et al. Spatial and temporal gene expression for fibroblast growth factor type I receptor (FGFR1) during fracture healing in the rat. Bone 2001;29:458–66. [PubMed: 11704499]
12. Nakajima A, Shimizu S, Moriya H, Yamazaki M. Expression of fibroblast growth factor receptor-3 (FGFR3), signal transducer and activator of transcription-1, and cyclin-dependent kinase inhibitor p21 during endochondral ossification: differential role of FGFR3 in skeletal development and fracture repair. Endocrinology 2003;144:4659–68. [PubMed: 12960068]
13. Rundle CH, Miyakoshi N, Ramirez E, Wergedal JE, Lau KH, Baylink DJ. Expression of the fibroblast growth factor receptor genes in fracture repair. Clin Orthop Relat Res 2002:253–63. [PubMed: 12360035]
14. Schmid GJ, Kobayashi C, Sandell LJ, Ornitz DM. Fibroblast growth factor expression during skeletal fracture healing in mice. Dev Dyn 2009;238:766–74. [PubMed: 19235733]
15. Murakami M, Simons M. Fibroblast growth factor regulation of neovascularization. Curr Opin Hematol 2008;15:215–20. [PubMed: 18391788]
16. Liu Z, Lavine KJ, Hung IH, Ornitz DM. FGF18 is required for early chondrocyte proliferation, hypertrophy and vascular invasion of the growth plate. Dev Biol 2007;302:80–91. [PubMed: 17014841]

17. Hung IH, Yu K, Lavine KJ, Ornitz DM. FGF9 regulates early hypertrophic chondrocyte differentiation and skeletal vascularization in the developing stylopod. Dev Biol 2007;307:300–13. [PubMed: 17544391]

18. Bonnarens F, Einhorn TA. Production of a standard closed fracture in laboratory animal bone. J Orthop Res 1984;2:97–101. [PubMed: 6491805]

19. Hiltunen A, Vuorio E, Aro HT. A standardized experimental fracture in the mouse tibia. J Orthop Res 1993;11:305–312. [PubMed: 8483044]

20. Holstein JH, Menger MD, Culemann U, Meier C, Pohlemann T. Development of a locking femur nail for mice. J Biomech 2007;40:215–9. [PubMed: 16376352]

21. Jepsen KJ, Price C, Silkman LJ, Nicholls FH, Nasser P, Hu B, et al. Genetic variation in the patterns of skeletal progenitor cell differentiation and progression during endochondral bone formation affects the rate of fracture healing. J Bone Miner Res 2008;23:1204–16. [PubMed: 18348700]

22. Grongroft I, Heil P, Matthys R, Lezuo P, Tami A, Perren S, et al. Fixation compliance in a mouse osteotomy model induces two different processes of bone healing but does not lead to delayed union. J Biomech 2009;42:2089–96. [PubMed: 19643416]

23. Danova NA, Colopy SA, Radtke CL, Kalscheur VL, Markel MD, Vanderby R, et al. Degradation of bone structural properties by accumulation and coalescence of microcracks. Bone 2003;33:197–205. [PubMed: 14499353]

24. Kidd LJ, Stephens AS, Kuliwaba JS, Fazzalari NL, Wu AC, Forwood MR. Temporal pattern of gene expression and histology of stress fracture healing. Bone. 2009

25. Tami AE, Nasser P, Schaffler MB, Knothe Tate ML. Noninvasive fatigue fracture model of the rat ulna. J Orthop Res 2003;21:1018–24. [PubMed: 14554214]

26. Uthgenannt BA, Silva MJ. Use of the rat forelimb compression model to create discrete levels of bone damage in vivo. J Biomech 2007;40:317–324. [PubMed: 16519891]

27. Colopy SA, Benz-Dean J, Barrett JG, Sample SJ, Lu Y, Danova NA, et al. Response of the osteocyte syncytium adjacent to and distant from linear microcracks during adaptation to cyclic fatigue loading. Bone 2004;35:881–91. [PubMed: 15454095]

28. Hsieh YF, Silva MJ. In vivo fatigue loading of the rat ulna induces both bone formation and resorption and leads to time-related changes in bone mechanical properties and density. Journal of Orthopaedic Research 2002;20:764–771. [PubMed: 12168665]

29. Uthgenannt BA, Kramer MH, Hwu JA, Wopenka B, Silva MJ. Skeletal self-repair: stress fracture healing by rapid formation and densification of woven bone. J Bone Miner Res 2007;22:1548–56. [PubMed: 17576168]

30. Bentolila V, Boyce TM, Fyhrie DP, Drumb R, Skerry TM, Schaffler MB. Intracortical remodeling in adult rat long bones after fatigue loading. Bone 1998;23:275–281. [PubMed: 9737350]

31. Wohl GR, Towler DA, Silva MJ. Stress fracture healing: Fatigue loading of the rat ulna induces upregulation in expression of osteogenic and angiogenic genes that mimic the intramembranous portion of fracture repair. Bone 2009;44:320–330. [PubMed: 18950737]

32. Ferguson VL, Ayersa RA, Bateman TA, Simske SJ. Bone development and age-related bone loss in male C57BL/6J mice. Bone 2003;33:387–398. [PubMed: 13678781]

33. Lee KC, Maxwell A, Lanyon LE. Validation of a technique for studying functional adaptation of the mouse ulna in response to mechanical loading. Bone 2002;31:407–412. [PubMed: 12231414]

34. Robling AG, Turner CH. Mechanotransduction in bone: genetic effects on mechanosensitivity in mice. Bone 2002;31:562–569. [PubMed: 12477569]

35. Deckers MM, van Bezooijen RL, van der Horst G, Hoogendam J, van Der Bent C, Papapoulos SE, et al. Bone morphogenetic proteins stimulate angiogenesis through osteoblast-derived vascular endothelial growth factor A. Endocrinology 2002;143:1545–53. [PubMed: 11897714]

36. Wang Y, Wan C, Deng L, Liu X, Cao X, Gilbert SR, et al. The hypoxia-inducible factor alpha pathway couples angiogenesis to osteogenesis during skeletal development. J Clin Invest 2007;117:1616–1626. [PubMed: 17549257]

37. Tsuji K, Bandyopadhyay A, Harfe BD, Cox K, Kakar S, Gerstenfeld L, et al. BMP2 activity, although dispensable for bone formation, is required for the initiation of fracture healing. Nat Genet 2006;38:1424–9. [PubMed: 17099713]

38. Wan C, Gilbert SR, Wang Y, Cao X, Shen X, Ramaswamy G, et al. Activation of the hypoxia-inducible factor-1alpha pathway accelerates bone regeneration. Proc Natl Acad Sci U S A 2008;105:686–91. [PubMed: 18184809]

39. Sample SJ, Behan M, Smith L, Oldenhoff WE, Markel M, Kalscheur VL, et al. Functional Adaptation to Loading of a Single Bone is Neuronally Regulated and Involves Multiple Bones. J Bone Miner Res 2008;23:1372–81. [PubMed: 18410233]

40. Sugiyama T, Price JS, Lanyon LE. Functional adaptation to mechanical loading in both cortical and cancellous bone is controlled locally and is confined to the loaded bones. Bone. 2009

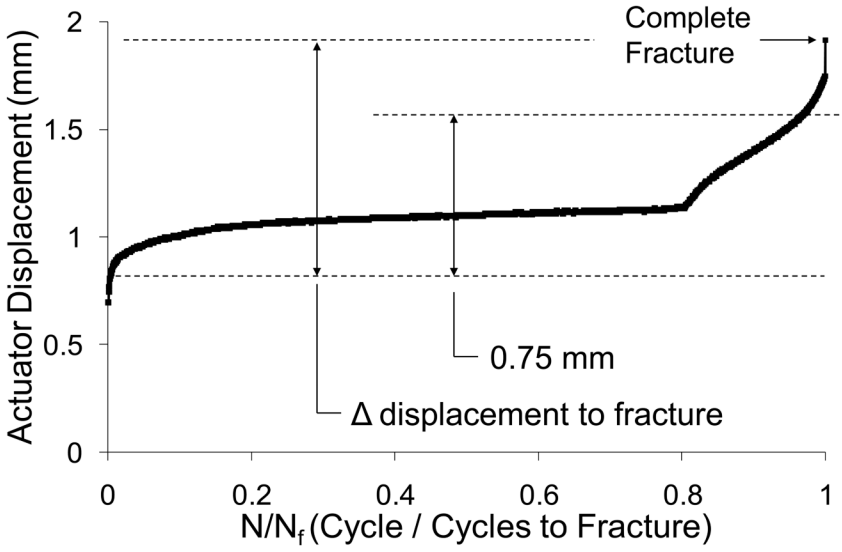

Figure 1.

Representative displacement history (peak displacement for each cycle) for fatigue loading to complete fracture of a mouse forelimb (2094 cycles to fracture). On average, fracture occurred when peak displacement increased by 1.25 ± 0.32 mm, relative to its value at cycle 10. For subsequent non-displaced fracture experiments, forelimbs were fatigue-loaded until peak displacement increased by 0.75 mm (60% of fracture).

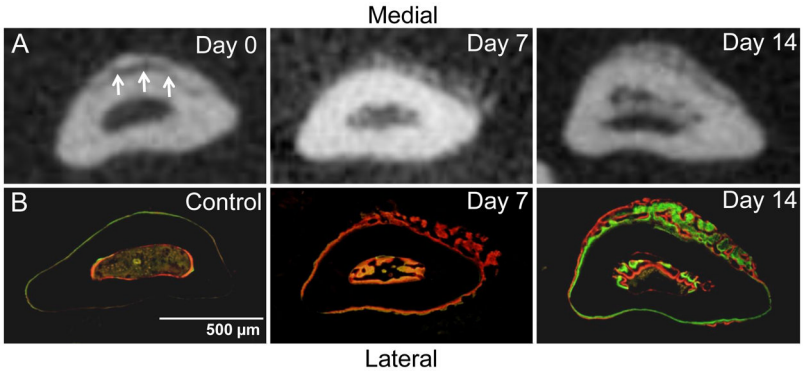

Figure 2.

Abundant woven bone formation near the site of non-displaced fracture. Transverse sections of ulnae (0–1 mm distal to mid-shaft) obtained by microCT (A) and fluorescent microscopy (B). The fracture is seen on the medial side of the ulna on day 0 microCT (arrows). Periosteal and endosteal woven bone is present at low density on day 7 and at higher density on day 14. The periosteal woven bone is thicker medially, corresponding to the fracture location. (Calcein green and alizarin complexone [red] were administered 7 and 2 days prior to sacrifice, respectively.)

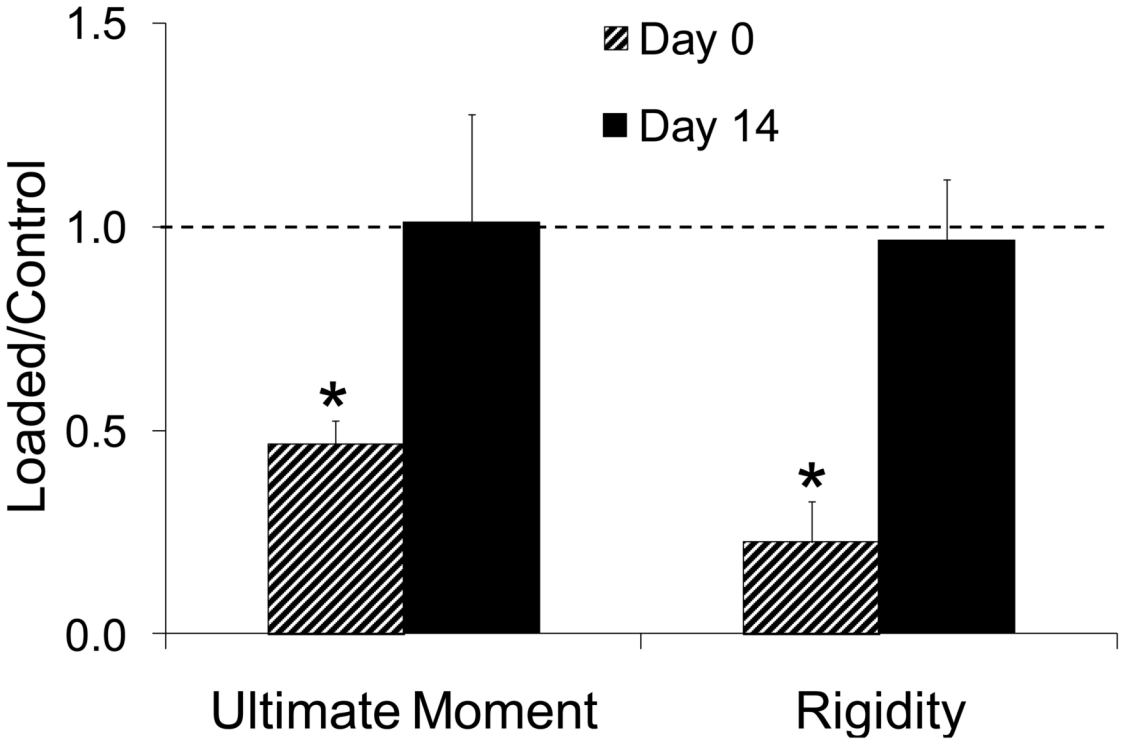

Figure 3.
Recovery of ulnar mechanical properties. Ultimate moment (a measure of strength) and rigidity (a measure of stiffness) were assessed by three-point bending. Loaded ulnae were 53% weaker and 77% less stiff than non-loaded controls on day 0, due to fatigue damage. By day 14, loaded ulnae had normal strength and stiffness. (mean ± SD)
* loaded different from non-loaded, contralateral control: paired t-test, $p < 0.05$

Figure 4A

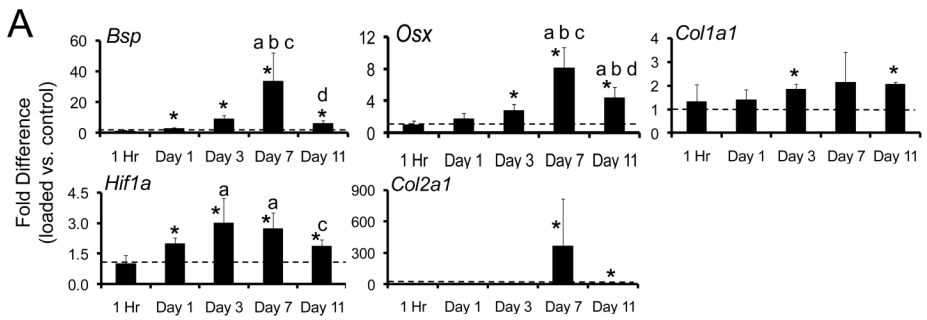

Figure 4B

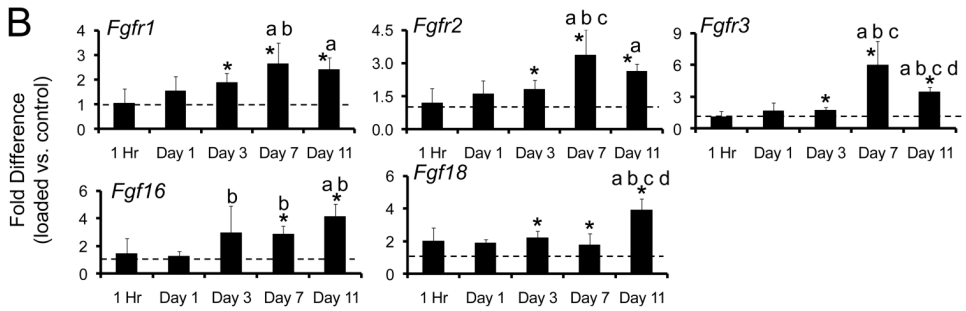

Figure 4.

Fatigue loading stimulated upregulation of (A) osteogenic, hypoxic and chondrogenic genes, and (B) FGF-family genes. Data represent fold-difference (mean ± SD) in expression levels of loaded ulnae compared to contralateral, non-loaded control ulnae (dashed line represents fold difference of 1). Shown are genes with a fold difference of greater than 2.

* loaded different from non-loaded, contralateral control: paired t-test, $p < 0.05$

[a] different than 1 Hour, [b] different than Day 1, [c] different than Day 3, [d] different than Day 7: ANOVA, $p < 0.05$

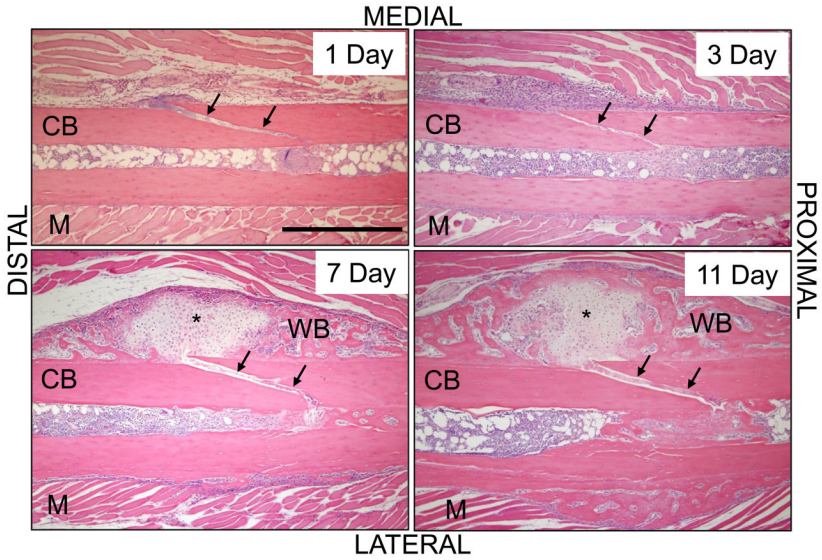

Figure 5.

Fatigue loading creates a non-displaced fracture and triggers a local periosteal response. Longitudinal sections of fatigue-loaded ulnae (H&E) show that the fracture occurred as a non-displaced, oblique crack through the medial cortex (arrows). On day 1 after loading, a clot is seen on both ends of the crack. On day 3, the periosteum is expanded and filled with cellular, fibrovascular tissue; nascent woven bone is seen sub-periosteally. On days 7 and 11 there is abundant woven bone on the medial periosteum. In approximately one-half of specimens the callus contained no cartilage (not shown), but in the others there was cartilage (*) in the center of the woven bone. [M] muscle; [CB] cortical bone; [WB] woven bone. Scale bar = 500 μm.

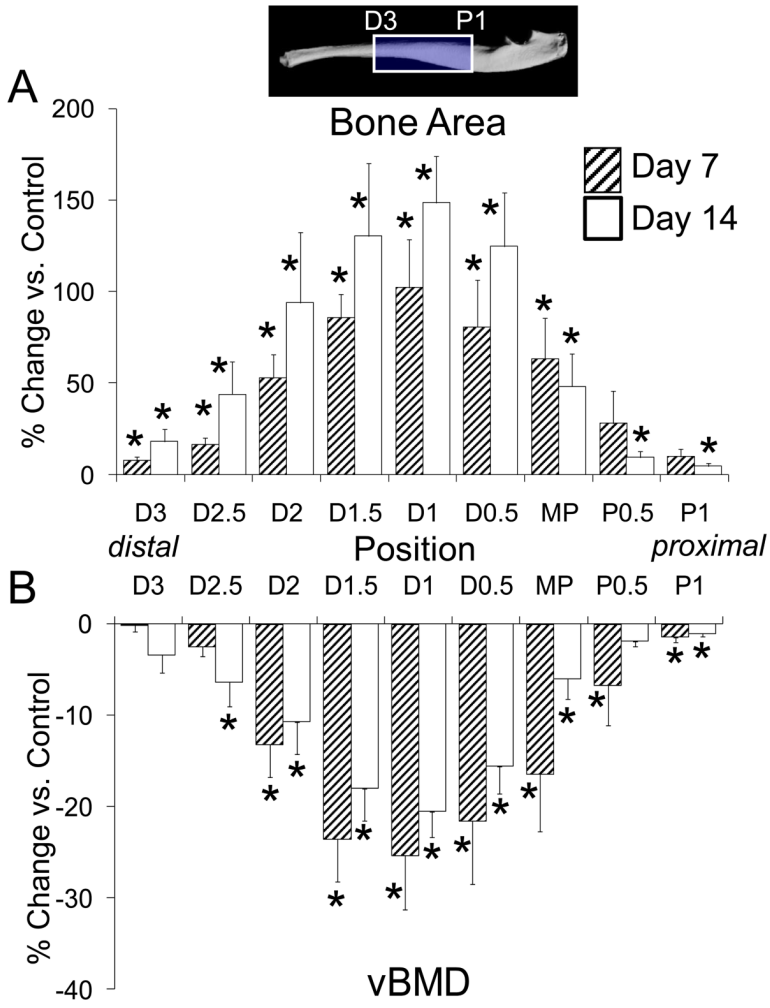

Figure 6.

Change in (A) bone area and (B) volumetric bone mineral density in loaded compared to control ulnae was determined by microCT at nine sections spanning 4 mm of the ulnar diaphysis. The peak increase in bone area was centered at section D1 (1 mm distal to midpoint [MP]), corresponding to the location of fracture, and diminished proximal and distal to this. BMD was decreased in a similar pattern, indicating the addition of lower density woven bone. (mean ± SE)

* loaded different from non-loaded, contralateral control: paired t-test, $p < 0.05$

Bone. Author manuscript; available in PMC 2011 June 1.

Table 1

Number of ulnae (right & left pairs) for each timepoint and outcome

Day	qPCR	Histology	Histomorphometry	Mechanical Testing	microCT[3]
0	5[1]	3	-	10	10
1	5[2]	3	-	-	-
3	5	3	-	-	-
7	5	3	8	-	8
11	4	3	-	-	-
14	-	-	8	13[4]	21[4]

An additional two mice were loaded but excluded due to complete fracture.

[1] One of these samples was excluded because it was a consistent outlier (+ 2 SD from mean).

[2] One of these samples was excluded because of problem with RNA quality.

[3] Ulnae used for histomorphometry and mechanical testing were first scanned by microCT.

[4] Two of these samples were not included in data analysis because a displaced fracture was observed on microCT.

Table 2

Target genes for expression analysis

Gene	Name	RefSeq (accession no.)	ABI catalog no.
Bmp2	Bone Morphogenetic Protein 2	NM_007553.2	Mm01340178_m1
Bsp	Bone sialoprotein	NM_008318.2	Mm00492555_m1
Osx	Osterix (Sp7)	NM_130458.3	Mm00504574_m1
Vegfa	Vascular Endothelial Growth Factor	NM_001025250.3, NM_001025257.3, NM_009505.4	Mm00437304_m1
Hif1a	Hypoxia-inducible factor 1α	NM_010431.2	Mm00468869_m1
Col1a1	Type I Collagen	NM_010155.3	Mm00468761_m1
Col2a1	Type II Collagen	NM_031163.2	Mm01309565_m1
Fgfr1	Fibroblast Growth Factor Receptor 1	NM_001079908.1, NM_010206.2	Mm00438923_m1
Fgfr2	Fibroblast Growth Factor Receptor 2	NM_201601.2, NM_010207.2	Mm00438941_m1
Fgfr3	Fibroblast Growth Factor Receptor 3	NM_008010.3	Mm00433294_m1
Fgf1	Fibroblast Growth Factor 1	NM_010197.3	Mm00438906_m1
Fgf2	Fibroblast Growth Factor 2	NM_008006.2	Mm00433287_m1
Fgf9	Fibroblast Growth Factor 9	NM_013518.3	Mm00442795_m1
Fgf16	Fibroblast Growth Factor 16	NM_030614.2	Mm00651404_m1
Fgf18	Fibroblast Growth Factor 18	NM_008005.1	Mm00433286_m1

Table 3

Ulnar mechanical properties determined by three-point bending post mortem (mean ± SD)

	Ultimate Moment (N×mm)		Rigidity (N×mm^2)		Normalized Post Yield Displacement (mm/mm^2)		Normalized Fracture Energy (N)	
	Control	**Loaded**	**Control**	**Loaded**	**Control**	**Loaded**	**Control**	**Loaded**
Day 0 (n=10)	5.3 ± 0.6	2.5 ± 0.3*	100.4 ± 16.2	21.7 ± 6.7*	0.14 ± 0.05	0.11 ± 0.06	0.65 ± 0.15	0.39 ± 0.10*
Day 14 (n=11)	6.0 ± 0.6	6.0 ± 1.7	120.2 ± 22.9	113.3 ± 11.3	0.16 ± 0.03	0.10 ± 0.08	0.75 ± 0.13	0.73 ± 0.51

*loaded different from non-loaded, contralateral control: paired t-test, $p < 0.05$

Table 4

Fold difference in expression of target genes in loaded ulnae versus control (mean ± SD).

Gene	1 Hour	Day 1	Day 3	Day 7	Day 11
Bmp2	1.6 ± 0.8	1.9 ± 0.6*	1.1 ± 0.6	1.9 ± 0.6*	1.7 ± 0.3*
Bsp	1.1 ± 0.6	2.8 ± 0.7*	8.8 ± 2.5*	33 ± 19*a b c	6.1 ± 2.0*d
Osx	0.9 ± 0.5	1.7 ± 0.7	2.8 ± 0.8*	8.1 ± 2.6*a b c	4.4 ± 1.4*a b d
Vegfa	1.0 ± 0.4	1.1 ± 0.3	0.8 ± 0.4	0.9 ± 0.4	1.3 ± 0.2*
Hif1a	1.0 ± 0.4	2.0 ± 0.3*	3.0 ± 1.2*a	2.7 ± 0.8*a	1.9 ± 0.3*c
Col1a1	1.3 ± 0.7	1.4 ± 0.4	1.9 ± 0.2*	2.1 ± 1.3	2.1 ± 0.1*
Col2a1	0.8 ± 0.3	0.7 ± 0.7	1.1 ± 0.9	363 ± 458*	6.2 ± 5.7*
Fgfr1	1.1 ± 0.6	1.5 ± 0.6	1.9 ± 0.4*	2.6 ± 0.9*a b	2.4 ± 0.5*a
Fgfr2	1.2 ± 0.7	1.6± 0.6	1.8 ± 0.4*	3.4 ± 1.2*a b c	2.6 ± 0.3*a
Fgfr3	1.1 ± 0.6	1.7 ± 0.7	1.7 ± 0.3*	6.0 ± 2.2*a b c	3.4 ± 0.5*a b c d
Fgf1	0.8 ± 0.2	1.0 ± 0.4	0.6 ± 0.5	0.8 ± 0.3	1.2 ± 0.4
Fgf2	1.1 ± 0.4	1.8 ± 0.7	1.6 ± 0.5	1.3 ± 0.4	1.8 ± 0.2*
Fgf9	1.0 ± 0.5	0.7 ± 0.6	0.7 ± 0.5	0.7 ± 0.3	1.5 ± 0.3*b c d
Fgf16	1.4 ± 1.1	1.2 ± 0.4	3.0 ± 1.9	2.9 ± 0.6*	4.1 ± 0.9*
Fgf18	2.0 ± 0.8	1.9 ± 0.2	2.2 ± 0.4*	1.8 ± 0.6*	3.9 ± 0.78a b c d

*loaded different from non-loaded, contralateral control: paired t-test, $p < 0.05$

*a*different than 1 Hour,

*b*different than Day 1,

*c*different than Day 3,

*d*different than Day 7: ANOVA, $p < 0.05$

Table 5

Dynamic histomorphometric indices of bone formation in loaded ulnae compared to control (mean ± SD)

	Single Labeled Surface (%)	Double Labeled Surface (%)	Woven Bone Labeled Surface (%)	Non Labeled Surface (%)	Woven Bone Area (mm^2)	Total Bone Area (mm^2)
Control	5.3 ± 7.6	0.1 ± 0.4	0.0 ± 0.0	94.6 ± 7.7	0.0 ± 0.0	0.245 ± 0.021
Day 7	14.8 ± 18.7	0.0 ± 0.0	57.2 ± 21.9[a]	28.0 ± 12.3[a]	0.022 ± 0.009[a]	0.275 ± 0.018[a]
Day 14	14.9 ± 12.6	27.2 ± 7.3[a b]	41.8 ± 27.5[a]	16.1 ± 12.9[a b]	0.017 ± 0.013[a]	0.292 ± 0.034[a]

Control group consists of non-loaded ulnae from day 7 and 14 mice, pooled.

[a] different than Control,

[b] different than Day 7: ANOVA, $p < 0.05$